Meccanica (2015) 50:1205–1216
DOI 10.1007/s11012-014-0007-x

Photo-disintegration of the iron nucleus in fractured magnetite rocks with magnetostriction

A. Widom · J. Swain · Y. N. Srivastava

Received: 13 January 2014 / Accepted: 23 June 2014 / Published online: 19 August 2014

Abstract There has been considerable interest in recent experiments on iron nuclear disintegrations observed when rocks containing such nuclei are crushed and fractured. The resulting nuclear transmutations are particularly strong for the case of magnetite rocks, i.e. loadstones. We argue that the fission of the iron nucleus is a consequence of photo-disintegration. The electro-strong coupling between electromagnetic fields and nuclear giant dipole resonances are central for producing observed nuclear reactions. The large electron energies produced during the fracture of piezomagnetic rocks are closely analogous to the previously discussed case of the fracture of piezoelectric rocks. In both cases electro-weak interactions can produce neutrons and neutrinos from energetic protons and electrons thus inducing nuclear transmutations. The electro-strong condensed matter coupling discussed herein represents new many body collective nuclear photo-disintegration effects.

Keywords 62.20.mm · 81.40.Np · 03.75.Be · 14.20.Dh

A. Widom · J. Swain
Physics Department, Northeastern University, Boston, MA, USA

Y. N. Srivastava (✉)
Physics Department & INFN, University of Perugia, Perugia, Italy
e-mail: yogendra.srivastava@gmail.com

1 Introduction

Recent measurements of nuclear reactions [1–3] that accompany the fracturing [4–7] of piezoelectric and piezomagnetic rocks have inspired a great deal of interest. The contribution of electro-weak processes to the production of neutrons,

$$e^- + p^+ \rightarrow n + \nu_e, \tag{1}$$

during the fracture of piezoelectric rocks has been discussed in previous work [8]. One of the purposes of this work is to expand the theory to include the fracture of rocks [9] with magnetostriction, again employing the conversion of mechanical energy (phonons) to electromagnetic energy (photons) and vice-versa.

Our purpose is also to investigate other sources of nuclear radiation, in particular those radiations that are a consequence of electro-strong [10, 11] nuclear fission reactions. To see what is involved, consider the fracture of Fe_3O_4 magnetite rocks, i.e. magnetic semiconductor loadstones. The fracture process accelerates electrons which in turn produce electromagnetic radiation. Such radiation can induce the photo-disintegration of the iron nucleus. The absorption of a photon can cause a transition to an excited compound nuclear state, e.g.

$$\gamma + {}^{56}\mathrm{Fe} \rightarrow {}^{56}\mathrm{Fe}^{*} \tag{2}$$

The quantum electrodynamic excitation to a compound nuclear state is exhibited in the Feynman diagrams of Fig. 1. The photon nuclear vertex

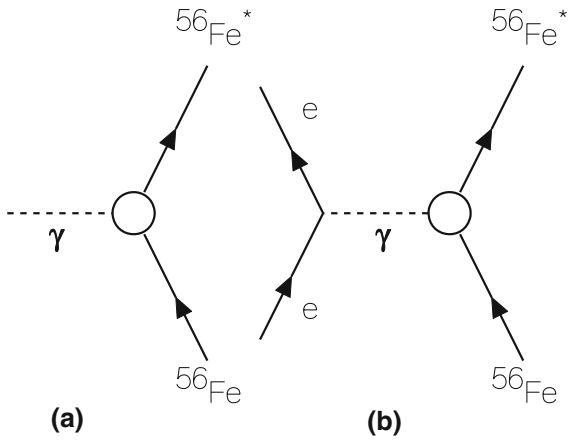

Fig. 1 Shown in **a** is the Feynman diagram for producing an excited compound nucleus from a real Bremsstrahlung photon. Shown in **b** is a similar process due to an incident electron exchanging a virtual photon with the nucleus

coupling is via the iron nucleus giant dipole resonance [12]. The strong interactions control the decay of the compound nucleus

$$^{56}\mathrm{Fe}^{*} \rightarrow (\text{fission products}). \tag{3}$$

In general terms, the photo-disintegration of nuclei is presently well understood.

In Sect. 2 the giant dipole resonant coupling to the electromagnetic field is reviewed. The total cross section for absorbing the photon in Fig. 1a has a peak value of

$$\sigma_0 = 4\pi Z\alpha\left(\frac{\hbar}{M\Gamma}\right), \tag{4}$$

wherein $Z = 26$ is the number of protons in the iron nucleus, the quantum electrodynamic coupling strength is $\alpha = (e^2/\hbar c) \approx 1/137.036$, the proton mass is M and the fission decay rate of the compound nucleus in Eq. (3) is Γ. The silicon and aluminum photo-disintegration fission channels are briefly discussed in Sect. 3.

In Sect. 4 we consider the retarding force

$$\bar{F} = -\frac{dE}{dx}, \tag{5}$$

or energy loss per unit length for an energetic electron passing through magnetite. The ratio of how much energy dE is lost to other electrons in atomic transitions and how much energy $d\tilde{E}$ is lost to giant dipole excitations of the compound nucleus is computed in detail. Formally, the energy transfer efficiency $\eta = (d\tilde{E}/dE) \sim 1\%$.

In Sect. 5 a theoretical explanation is provided for the experimental evidence that fracturing loadstones produces photo-disintegration fission products of ^{56}Fe nuclei. The elastic energy of mesoscopic microcrack production during a fracture ultimately yields a major macroscopic fracture separation. The mechanical energy is converted by magnetostriction into electromagnetic field energy. The electromagnetic field energy decays via radio frequency (microwave) oscillations. The radio frequency fields accelerate the condensed matter electrons which then collide with nuclei producing fission products on the surfaces of these microcracks. In the concluding Sect. 6, the nature of fission microcrack wall remnants are discussed.

2 Giant dipole resonances

Over several decades, virtual photons from electron scattering as well as Bremmstrahlung photons have been routinely used to cause nuclear photo-disintegration via the generation of giant dipole resonances (GDR) in the intermediate state [13, 14]. The reactions studied extensively are with production of one or two neutrons such as $A(\tilde{\gamma}, n)A^{*}$ and $A(\tilde{\gamma}, nn)A^{**}$, where $\tilde{\gamma}$ is the virtual photon from electron scattering and the final nuclei, $[A^{*}, A^{**}]$ stand for the disintegration product collectively. Of course, their counterpart nuclear breakup reactions $A(\gamma, n)A^{*}$ and $A(\gamma, nn)A^{**}$ from real Bremmstrahlung photons (γ) have also been of continued interest and study. Typically, GDRs are in the $(10 \div 20)$ MeV range for heavy nuclei and $(15 \div 25)$ MeV for light nuclei. Detailed compendia of such data exist [15] given their importance for a variety of practical applications e.g., in producing radio-isotopes for medicinal purposes [16, 17].

In this section, we describe the theoretical formalism leading to our explanation of the experimental results on iron nuclear disintegrations observed when rocks containing such nuclei are crushed and fractured. The fission of the iron nucleus occurs as a consequence of a photo-disintegration process. In the case of the fracture of Fe_3O^4 magnetite rocks, the accelerated electrons produced by the fracture, yield a very intense electromagnetic field. This radiation field

induces in turn the photo-excitation of the iron nucleus from its ground state ^{56}Fe to an excited state ^{56}Fe*. This excited state of iron, ^{56}Fe* , can disintegrate through strong interactions in different channels. For the other component of magnetite ^{16}O, an analogous excitation is produced by the radiation field to its excited state ^{16}O*, the latter subsequently also disintegrates via strong interactions.

Below, the essential steps of the calculation and the results for the photo-excitation of a giant dipole resonance are given. In (2.1), the dipole Hamiltonian is written down and frequency dependent nuclear polarizability $\beta(\zeta)$ defined. In (2.2), expressions for the elastic and total photo-nuclear cross-sections for ^{56}Fe are shown in terms of $\beta(\zeta)$. In (2.3), a dispersion relation and second order perturbation theory are used to derive a sum rule that relates the static value of the nuclear polarizability $\beta(0)$ to the total photo-nuclear cross-section. In (2.4), a very often used, single giant dipole resonance model is discussed. Semi-quantitative estimates for the model parameters are made through the Migdal zero sound expressions from Fermi-Landau liquid theory in the last part (2.5) of this section.

2.1 Nuclear polarizability

Let $|0\rangle = |^{56}\mathrm{Fe}\rangle$ represent the ground state internal wave function of the iron nucleus. Representing the dipole approximation for the interaction in Fig. 1,

$$H_{\mathrm{int}} = -\mathbf{E}\cdot\mathbf{d}, \tag{6}$$

the nuclear polarizability

$$\beta(\zeta) = \frac{i}{3\hbar}\int_0^\infty e^{i\zeta t}\langle 0|\mathbf{d}(t)\cdot\mathbf{d}(0) - \mathbf{d}(0)\cdot\mathbf{d}(t)|0\rangle dt. \tag{7}$$

The ground state of the ^{56}Fe nucleus has zero spin. The polarizability is thereby an isotropic tensor.

2.2 Photon cross sections

The elastic photon scattering amplitude for

$$\gamma + {}^{56}\mathrm{Fe} \rightarrow \gamma + {}^{56}\mathrm{Fe} \tag{8}$$

is given by

$$\mathcal{F}_{fi}(\omega) = \left(\frac{\omega}{c}\right)^2 \beta(\omega + i0^+)\mathbf{e}_\mathbf{f}^*\cdot\mathbf{e}_\mathbf{i} \tag{9}$$

wherein $\mathbf{e_{i,f}}$ are, respectively, the initial and final photon polarization vectors and ω is the photon frequency. The elastic photon cross section is thereby

$$\begin{aligned}\sigma_{\mathrm{el}}(\omega) &= \frac{1}{2}\sum_f\sum_i\int |\mathcal{F}_{fi}(\omega)|^2 d\Omega_f \ ,\\ \sigma_{\mathrm{el}}(\omega) &= \frac{8\pi}{3}\left(\frac{\omega}{c}\right)^4 |\beta(\omega+i0^+)|^2.\end{aligned} \tag{10}$$

wherein we have averaged over initial polarization states and summed over final polarization states. The total cross section follows from the optical theorem

$$\begin{aligned}\sigma_{\mathrm{tot}}(\omega) &= \left(\frac{4\pi c}{\omega}\right)\Im\mathfrak{m}\mathcal{F}_{ii}(\omega),\\ \sigma_{\mathrm{tot}}(\omega) &= \left(\frac{4\pi\omega}{c}\right)\Im\mathfrak{m}\beta(\omega+i0^+).\end{aligned} \tag{11}$$

The inelastic cross section $\sigma_{\mathrm{in}}(\omega)$ for the central reaction

$$\gamma + {}^{56}\mathrm{Fe} \rightarrow {}^{56}\mathrm{Fe}^* \rightarrow (\text{fission products}) \tag{12}$$

follows from Eqs. (10) and (11) via the sum rule

$$\sigma_{\mathrm{tot}}(\omega) = \sigma_{\mathrm{el}}(\omega) + \sigma_{\mathrm{in}}(\omega). \tag{13}$$

2.3 Dispersion relations

From Eq. (7), it is expected that the nuclear polarizability obey a dispersion relation for $\Im\mathfrak{m}\ \zeta > 0$ of the form

$$\beta(\zeta) = \frac{2}{\pi}\int_0^\infty\left[\frac{\omega\Im\mathfrak{m}\beta(\omega+i0^+)d\omega}{\omega^2-\zeta^2}\right]. \tag{14}$$

With

$$\hbar\omega_{n0} = E_n - E_0 \quad \text{and} \quad \mathbf{d}_{n0} = \langle n|\mathbf{d}|0\rangle, \tag{15}$$

we have

$$\Im\mathfrak{m}\beta(\omega+i0^+) = \frac{\pi}{3\hbar}\sum_n |\mathbf{d}_{n0}|^2\delta(\omega-\omega_{n0}) \tag{16}$$

For example, the static polarizability of the nucleus is given by

$$\beta = \lim_{\zeta\rightarrow i0^+}\beta(\zeta) = \frac{2}{\pi}\int_0^\infty \Im\mathfrak{m}\beta(\omega+i0^+)\frac{d\omega}{\omega}\ . \tag{17}$$

Employing Eq. (6) in second order perturbation theory

$$\frac{1}{2}\beta|\mathbf{E}|^2 = \sum_n \frac{|\langle n|H_{\rm int}|0\rangle|^2}{E_n - E_0}\ ,$$
$$\beta = \frac{2}{3\hbar}\sum_n \frac{|\mathbf{d}_{n0}|^2}{\omega_{n0}}\ . \tag{18}$$

For a nucleus of charge Z, the equal time commutation relation

$$\frac{i}{3\hbar}\left(\dot{\mathbf{d}}\cdot\mathbf{d} - \mathbf{d}\cdot\dot{\mathbf{d}}\right) = \frac{Ze^2}{M}, \tag{19}$$

wherein M is the proton mass, yields in virtue of Eqs. (7) and (19) the large frequency limit

$$\lim_{|\zeta|\to\infty} \zeta^2\beta(\zeta) = -\left(\frac{Ze^2}{M}\right). \tag{20}$$

Equations (14) and (20) imply the sum rule [18–20]

$$\frac{2}{\pi}\int_0^\infty \omega\Im\mathrm{m}\beta(\omega + i0^+)d\omega = \frac{Ze^2}{M}\ , \tag{21}$$

or equivalently

$$\int_0^\infty \sigma_{\rm tot}(\omega)d\omega = 2\pi^2\left(\frac{Ze^2}{Mc}\right) = 2\pi^2 Z\alpha\left(\frac{\hbar}{M}\right). \tag{22}$$

The above dispersion relation and sum rule are implemented in simple nuclear giant dipole resonant models.

2.4 Single giant resonance model

The most simple model for discussing the nuclear giant dipole resonance involves a single damped harmonic oscillator with resonant frequency ω_0 and damping coefficient Γ.

$$\beta(\zeta) = \frac{Ze^2}{M\left(\omega_0^2 - \zeta^2 - i\zeta\Gamma\right)}\ . \tag{23}$$

Equations (11) and (23) then imply a total cross section

$$\sigma_{\rm tot}(\omega) = \left(\frac{4\pi Ze^2}{Mc}\right)\left[\frac{\omega^2\Gamma}{\left(\omega_0^2 - \omega^2\right)^2 + \omega^2\Gamma^2}\right],$$
$$\sigma_{\rm tot}(\omega) = \sigma_0\left[\frac{\omega^2\Gamma^2}{\left(\omega_0^2 - \omega^2\right)^2 + \omega^2\Gamma^2}\right], \tag{24}$$
$$\sigma_0 = \left(\frac{4\pi Ze^2}{Mc\Gamma}\right) = 4\pi Z\alpha\left(\frac{\hbar}{M\Gamma}\right).$$

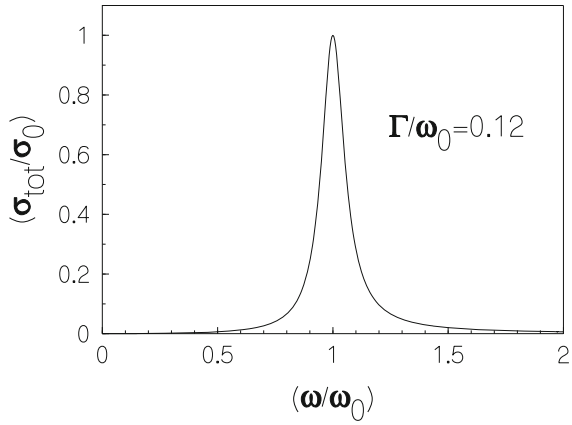

Fig. 2 Shown is the total cross section employing a single nuclear dipole giant resonance model according to Eq. (24). The resonant energy for creating a compound nucleus is $\hbar\omega_0$ as in Eq. (2). The transition rate is Γ for the compound nucleus to decay into fission products as in Eq. (3). The peak cross section is $\sigma_0 = 4\pi Z\alpha\hbar/M\Gamma$. The resonant width $\Gamma \approx 0.12\ \omega_0$ for ^{56}Fe is only approximate

The single resonance Eq. (24) is plotted in Fig. 2.

2.5 Model parameters

In the Migdal theory [21, 22] of the nuclear Landau–Fermi liquid, an isotopic spin zero sound mode of velocity c_0 confined to a spherical cavity has a frequency

$$\omega_0 = \frac{zc_0}{R} \quad (\text{with the lowest root of } z = \tan z > 0). \tag{25}$$

The radii of nuclei obey

$$R \approx r_0 A^{1/3} \quad \text{wherein} \quad r_0 \approx 1.2\ \text{fm}. \tag{26}$$

With the ratio of zero sound speed to light speed given by $(c_0/c) \approx 0.1$ we then have the prediction

$$\hbar\omega_0 \approx \frac{70\ \text{MeV}}{A^{1/3}} \quad \Rightarrow \quad \hbar\omega_0(^{56}\text{Fe}) \approx 20\ \text{MeV}. \tag{27}$$

Since the Landau–Fermi liquid theory gives rise to the complex zero sound mode frequency $\varpi = c_0 k - (i/2)Dk^2$ as $k \to 0$, the width of the zero sound resonance must have the form

$$\Gamma = D\left(\frac{\omega_0}{c_0}\right)^2 = \frac{z^2 D}{R^2} = \frac{\Gamma_0}{A^{2/3}} \tag{28}$$

wherein

$$\Gamma_0 = \left(\frac{z^2 D}{r_0^2}\right). \tag{29}$$

Thus,

$$\frac{\Gamma}{\omega_0} = \left(\frac{zD}{c_0 r_0}\right)\frac{1}{A^{1/3}} \approx \frac{0.5}{A^{1/3}}\ . \tag{30}$$

The above estimates are semi-quantitative but to the best of our knowledge are new.

3 Disintegration fission channels

In the photo-disintegration of iron

$$\gamma + {}^{56}\mathrm{Fe} \rightarrow {}^{56}\mathrm{Fe}^* \rightarrow (\text{fission products}). \tag{31}$$

one should consider the silicon and aluminum fission products within the prominent decay channels. If in accordance with the liquid drop model, the decay of the compound excited nucleus ^{56}Fe* is preferentially into two equal excited aluminum droplets, the decay reads

$${}^{56}\mathrm{Fe}^* \rightarrow 2\ {}^{28}\mathrm{Al}^*. \tag{32}$$

Each of the resulting aluminum nuclei, then undergoes the weak decay

$${}^{28}\mathrm{Al}^* \rightarrow {}^{28}\mathrm{Si} + e^- + \bar{\nu}_e. \tag{33}$$

Altogether,

$$\gamma + {}^{56}\mathrm{Fe} \rightarrow 2\ {}^{28}\mathrm{Si} + 2e^- + 2\bar{\nu}_e \quad (\text{two Si channel}). \tag{34}$$

If two neutrons evaporate from each of the two resulting aluminum nuclei

$${}^{28}\mathrm{Al}^* \rightarrow {}^{27}\mathrm{Al} + n, \tag{35}$$

then a possible channel is

$$\gamma + {}^{56}\mathrm{Fe} \rightarrow 2\ {}^{27}\mathrm{Al} + 2n \quad (\text{two Al channel}). \tag{36}$$

A third channel is evidently

$$\gamma + {}^{56}\mathrm{Fe} \rightarrow {}^{27}\mathrm{Al} + {}^{28}\mathrm{Si} + n + e^- + \bar{\nu}_e\ , \quad (\mathrm{Al} + \mathrm{Si}\ \text{channel}). \tag{37}$$

In terms of the branching ratio,

$$b = \frac{\Gamma\left({}^{28}\mathrm{Al}^* \rightarrow {}^{28}\mathrm{Si} + e^- + \bar{\nu}_e\right)}{\Gamma\left({}^{28}\mathrm{Al}^* \rightarrow {}^{27}\mathrm{Al} + n\right)}\ , \tag{38}$$

one should be able to compute the branching ratio of the above three fission products.

In magnetite Fe_3O_4, there will also be the photo-disintegration of the ^{16}O nucleus,

$$\gamma + {}^{16}\mathrm{O} \rightarrow {}^{16}\mathrm{O}^* \rightarrow (\text{fission products}). \tag{39}$$

Possible fission channels are thereby

$$\begin{aligned}
&{}^{16}\mathrm{O}^* \rightarrow {}^{15}\mathrm{O} + n,\\
&{}^{16}\mathrm{O}^* \rightarrow {}^{15}\mathrm{N} + p^+,\\
&{}^{16}\mathrm{O}^* \rightarrow {}^{14}\mathrm{N} + d^+,\\
&{}^{16}\mathrm{O}^* \rightarrow {}^{13}\mathrm{N} + t^+,\\
&{}^{16}\mathrm{O}^* \rightarrow {}^{13}\mathrm{C} + {}^{3}\mathrm{He},\\
&{}^{16}\mathrm{O}^* \rightarrow {}^{12}\mathrm{C} + \alpha,\\
&{}^{16}\mathrm{O}^* \rightarrow {}^{10}\mathrm{B} + {}^{6}\mathrm{Li}.
\end{aligned} \tag{40}$$

The photo-disintegration of oxygen gives rise to diverse types of nuclear radiation.

4 Retardation forces

Consider a beam of electrons each having an energy

$$E = mc^2\gamma = \frac{mc^2}{\sqrt{1-(v/c)^2}}\ . \tag{41}$$

passing through magnetite. The energy loss per unit length for the electron is the retarding force

$$F = -\frac{dE}{dx}\ . \tag{42}$$

If the fast electron causes other electrons to undergo atomic transitions, then the retarding force takes on the well known form [23]

$$F = \left(\frac{4\pi n e^4}{mv^2}\right)\left[\ln\left(\frac{mv^2\gamma^2}{\hbar\omega_i}\right) - \left(\frac{v}{c}\right)^2\right], \tag{43}$$

wherein $\hbar\omega_i$ is the log mean ionization energy of an atom and n is the density of electrons per unit volume.

For $\tilde{n}$ iron ^{56}Fe nuclei per unit volume, the retardation force due to the giant dipole resonance at frequency ω_0 in iron is given by

$$\tilde{F} = \left(\frac{4\pi\tilde{n}Z^2e^4}{Mv^2}\right)\left[\ln\left(\frac{Mv^2\gamma^2}{\hbar\omega_0}\right) - \left(\frac{v}{c}\right)^2\right], \tag{44}$$

wherein M is the proton mass.

The photo-disintegration efficiency may be defined as

$$\eta = \left(\frac{\tilde{F}}{F}\right) = \left(\frac{d\tilde{E}}{dE}\right), \tag{45}$$

wherein $d\tilde{E}$ is the energy transferred from a fast electron to fission products and dE is the energy transferred from a fast electron to atomic electronic transitions. The ratio of the energy excitations is small $(\omega_i/\omega_0) \sim 10^{-7}$. Equations (43), (44) and (45) imply for $\gamma \gg 1$

$$\eta \approx \left(\frac{Z^2\tilde{n}m}{nM}\right)\left\{\frac{\ln[(Mv^2\gamma^2/\hbar\omega_0)] - (v/c)^2}{\ln[(mv^2\gamma^2/\hbar\omega_i)] - (v/c)^2}\right\}. \tag{46}$$

Typically, the nuclear yield is as expected of the order of $\eta \sim 1\,\%$.

5 Fractured magnetic rocks

The thermodynamic properties of magnetite Fe_3O_4 are determined by the energy per unit volume $u = u(s, \mathbf{w}, \mathbf{H})$ wherein s is the entropy per unit volume, $\mathbf{w}$ is the strain and $\mathbf{H}$ is the magnetic intensity

$$du = Tds + \sigma : d\mathbf{w} - \mathbf{M} \cdot d\mathbf{H}. \tag{47}$$

Magnetite at room temperature is a ferromagnet. Within a magnetic domain, one may formally define a piezomagnetic coefficient by the thermodynamic derivatives

$$\beta_{i,jk} = \left(\frac{\partial M_i}{\partial w_{jk}}\right)_{s,\mathbf{H}} = -\left(\frac{\partial \sigma_{jk}}{\partial H_i}\right)_{s,\mathbf{w}}. \tag{48}$$

These coefficients describe how strain can induce magnetization and how magnetic intensity can induce stress. Some implications of this conversion from mechanical energy into electromagnetic energy are quite striking. If a solid has an impact on the surface of a magnetostrictive material, then the resulting induced electric fields can measure the nature of the induced impact stress.

The piezomagnetic coefficients describe the conversion of phonons (mechanical vibrations) into magnons (magnetic energy). Since the magnetization yields the current density

$$\mathbf{J}_{\text{mag}} = c\ curl\mathbf{M}, \tag{49}$$

Maxwell's equations describe the manner that magnons radiate photons,

$$\mathbf{E}(\mathrm{r}, t) = -\left(\frac{1}{c}\right) curl \int \frac{\dot{\mathbf{M}}(\mathrm{r}', t - R/c)}{R}\, d^3\mathrm{r}',$$
$$\text{wherein} \quad R = |\mathrm{r} - \mathrm{r}'| \quad \text{and} \quad \frac{\partial \mathbf{M}(\mathrm{r}, \mathrm{t})}{\partial \mathrm{t}} \equiv \dot{\mathbf{M}}(\mathrm{r}, \mathrm{t}). \tag{50}$$

Under conditions of rock crushing [9], the magnetization changes give rise in the microcracks [24, 25] to microwave radiation as given by Eq. (50). Microwaves can in turn give rise to accelerated electrons with an energy γmc^2. Let us consider this in more detail.

5.1 Loadstone fractures

The formation of microcracks during fracture can be formulated in terms of the elastic properties of the solid [26–28]. Let σ_{bond} be the fracture stress calculated on the basis of chemical bonds. The chemical bond stress can be expressed in terms of the elastic properties of the crystal

$$\sigma_{\text{bond}} = \left[\frac{2\mathcal{E}}{\pi(1 - \nu^2)}\right], \tag{51}$$

wherein $\mathcal{E}$ is Young's modulus and ν is Poisson's ratio. The experimental tensile stress σ_F of a loadstone obeys

$$\sigma_F \ll \sigma_{\text{bond}} \tag{52}$$

due to the intrinsic surface tension of the microcrack walls.

For loadstone we have the following numerical estimates;

$$\sigma_{\text{bond}} \sim 10^{12}\ \frac{\text{erg}}{\text{cm}^3} \quad \text{and} \quad \sigma_F \sim 10^{10}\ \frac{\text{erg}}{\text{cm}^3}. \tag{53}$$

During the time of microcrack formation, the stress within the empty open sliver is determined in order of magnitude by the Maxwell pressure tensor; i.e.

$$\sigma_F \sim \frac{\overline{|\mathbf{E}|^2}}{4\pi} \Rightarrow \overline{|\mathbf{E}|^2} \sim 10^{11}\ \text{Gauss}^2. \tag{54}$$

One may now compute the energy of electrons formed near the microcrack walls due to electric field generation.

5.2 Electron energy

The rate of change of momentum of an electron in an electric field is given by

$$\frac{d\mathrm{p}}{dt} = e\mathbf{E}. \tag{55}$$

Putting

$$mc^2\gamma = \sqrt{c^4m^2 + c^2\overline{|\mathbf{p}|^2}}\ , \tag{56}$$

yields

$$\gamma^2 = 1 + \frac{\overline{|\mathbf{p}|^2}}{m^2c^2} = 1 + \frac{e^2\overline{|\mathbf{E}|^2}}{m^2c^2\Omega^2}\ , \tag{57}$$

wherein Eq. (55) has been invoked and Ω is an effective frequency of electric field fluctuations [8]

$$\frac{1}{\Omega^2} = \frac{\int |\mathbf{E}_\omega|^2(\mathbf{d}\omega/\omega^2)}{\int |\mathbf{E}_\omega|^2\mathbf{d}\omega}\ . \tag{58}$$

Since

$$\frac{e}{mc} = 1.75882915 \times 10^7 \left(\frac{1}{\text{Gauss sec}}\right), \tag{59}$$

Eqs. (54), (57) and (59) yield

$$\gamma \sim \frac{3 \times 10^{12}/\text{s}}{\Omega}\ . \tag{60}$$

For the microwave electromagnetic radiation within the microcrack, $\Omega \sim 10^{10}/\text{s}$ so that

$$\gamma \sim 300 \Rightarrow \gamma mc^2 \sim 150\ \text{MeV}. \tag{61}$$

Such energetic electrons are perfectly capable of inducing the photo-disintegration of nuclei.

While the above results about the acceleration of electrons and their subsequent role in the dynamics of piezo-electric & piezo-magnetic rock crushing described above and in [8, 10] have been considered above reproach, some concerns have been raised in the application of their role in producing neutrons in electrolytic cell plasma through the electron capture reaction $[\tilde{e}^- + p \rightarrow n + \nu_e]$ induced by the weak interaction. Given the importance of the capture reaction in inducing low energy nuclear transmutations in Mizuno cells, we discuss it in an Appendix at the end of this paper and show that the raised criticisms are essentially irrelevant and thus our results are sound and remain robust.

5.3 Electron deposition

One can determine the order of magnitude of the number of energetic electrons which arrive on the surface area of a microcrack wall during the formation. If n_s represents the number per unit area of excess electronic charges, then applying Gauss' law to the wall surface yields

$$4\pi e n_s = E_\perp, \tag{62}$$

wherein $E_\perp$ is the component of the electric field normal to the surface. Equations (54) and (62) yield the electronic deposition density per unit area

$$n_s \sim 3 \times 10^{13}/\text{cm}^2 \tag{63}$$

If the yield of nuclear fission events per deposited electron is a few percent, then the density of fission events per unit area on a newly formed microcrack wall is given by

$$\varpi_s \sim \frac{10^{12}\ \text{fission events}}{\text{cm}^2} \tag{64}$$

This is a sufficient number of fission events for forming visible patches of monolayer films that would be observable to the eye.

6 Conclusions

The recent experimental work on nuclear radiations from fracturing magnetite, $[Fe_2^{+++}][Fe^{++}][O_4^{--}]$, can be largely understood. The theory contains an important electro-strong interaction component. Giant dipole resonances in the iron and oxygen nuclei

$$\gamma + {}^{56}\text{Fe} \rightarrow {}^{56}\text{Fe}^* \quad \text{and} \quad \gamma + {}^{16}\text{O} \rightarrow {}^{16}\text{O}^* \tag{65}$$

give rise to a conferable diversity of fission nuclear radiation from the excited compound nuclear states ^{56}Fe* and ^{16}O* when rocks containing such nuclei are crushed and fractured. Nuclear transmutations are present in the fracture of many brittle rocks but they are particularly plentiful for the case of magnetite rocks, i.e. loadstones. The fission event nuclei are a consequence of photo-disintegration. The electro-strong coupling between electromagnetic fields in piezomagnetic rocks are closely analogous to the previously discussed case of the fracture of piezoelectric rocks. In both cases, electro-weak interactions can

produce long wavelength neutrons and neutrinos from energetic protons and electrons thus inducing nuclear transmutations. The electro-strong condensed matter coupling discussed herein represents new many body collective nuclear photo-disintegration effects.

Appendix: Weak interactions

In years past we have been working on electro-weak interaction inverse beta decay [29–31] including electromagnetic interactions with collective plasma modes of motion. We have applied this theory to electron capture in a water plasma to explain observed nuclear transmutations on the cathode of a chemical cell [32].

Electron capture

Employing the electro-weak interaction wherein a heavy electron is captured by a nucleus to produce an added neutron and a neutrino, the electron capture rate for fully ionized plasmas can be computed if physical kinetic theory is employed in the following manner. (i) Consider the following reactions

$$\begin{aligned} &\text{(general)} \quad e^- + {}^{A}_{Z}X \rightarrow {}^{A}_{(Z-1)}X + \nu_e \\ &\text{(special case)} \quad \tilde{e}^- + p^+ \rightarrow n + \nu_e, \end{aligned} \tag{66}$$

wherein $\tilde{e}^-$ is an electron dressed by an external electromagnetic field. (ii) In the vacuum, the scattering amplitude for *small* relative velocity v between the electron and the target is described by a complex scattering length

$$\mathcal{F} = a + ib, \tag{67}$$

yielding an elastic and a total cross section given respectively by

$$\sigma_{el} = 4\pi(a^2 + b^2) \quad \sigma_{tot} = \frac{4\pi\Im\mathrm{m}\mathcal{F}}{k} = \frac{4\pi\hbar b}{\mu v} \tag{68}$$

wherein $\mu = mM/(m+M)$ is the reduced mass of the electron. (iii) The electron capture rate per scattering center in a two component neutral plasma is then

$$\Gamma = \left(\lim_{v\to 0} v\sigma_{tot}\right)\bar{n} = \left(\frac{4\pi\hbar b}{\mu}\right)\bar{n}. \tag{69}$$

(iv) The density of electrons with positions $\{\mathbf{r_j}\}$ sitting right on top of a given nucleus at position $\{\mathbf{R}\}$ is described by an equilibrium correlation function,

$$\bar{n} = \left\langle \sum_j \delta(\mathbf{R} - \mathbf{r_j}) \right\rangle. \tag{70}$$

Within the context of kinetic theory, which was not quite the many body quantum field theoretical approach taken in the original work [29], the central results are here given by Eqs. (69) and (70). It is the evaluation of Eq. (70) which has caused some controversy between us and with other workers at the University of Rome.

Electron correlation density $\bar{n}$

The computation of $\bar{n}$ made by the Rome University group [33] employed the zero temperature Hydrogen atomic bound state wave function at the origin

$$\bar{n} = |\psi_{bound}(0)|^2 = \frac{1}{\pi a_B^3}\ , \tag{71}$$

wherein a_B is the Bohr radius. Employing Eq. (5.3), Maiani *et al.* [33] calculated a rate smaller than that of our previous theory [29] by two orders of magnitude. We advised [34] the Rome group to calculate the correlation function in Eq. (70) employing a statistical ensemble at temperature$T \sim$ 5,000 K as in our previous theoretical work [29] but the Rome group took no notice of our reply to their calculation. We then pointed out more strongly that computing the rate using the ground state of Hydrogen was absurd because in the experiment the water plasma was so hot that it lighted up the laboratory. If the erroneous ground state computation of the Maiani et al. Eq. (71) held true, then the optical radiation would be virtually zero rather than blindingly bright. We further went on to show the Rome group how they should have approximately computed $\bar{n}$ for finite temperature. We employed Coulomb scattering state wave functions [35] for the fully ionized hot experimental [31] plasma. We found a substantially enhanced neutron production rate. The scattering wave function should replace the bound state wave function for estimates of the enhanced neutron production rate on water plasma drenched cathodes of chemical cells. Our purpose was to point out the source of this difference so that the physical principles may be resolved. Let us here present that calculation.

One must—for the physical plasma—employ the equation for $\bar{n}$ the hot temperature fully ionized dilute neutral plasma result for protons and electrons

$$\bar{n}_T = n\left\langle |\psi_{\mathbf{k}}(0)|^2 \right\rangle, \tag{72}$$

wherein T is the temperature, n is the number of electrons per unit volume averaged over the entire volume, $\psi_{\mathbf{k}}(\mathbf{r})$ is the Coulomb scattering wave function normalized to a non-scattering plane wave $\psi^0_{\mathbf{k}}(\mathbf{r}) = \exp(i\mathbf{k}\cdot\mathbf{r})$ and the thermal average is with respect to the Maxwell velocity distribution

$$\exp\left(-\frac{\hbar^2 k^2}{2\mu k_B T}\right) = \exp\left(-\frac{\mu v^2}{2k_B T}\right). \tag{73}$$

The standard mathematical expression [36] for the scattering of an electron off a proton is given by

$$\psi_{\mathbf{k}}(\mathbf{r}) = e^{i\mathbf{k}\cdot\mathbf{r}}\left[e^{\pi/2ka_B}\Gamma\left(1-\frac{i}{ka_B}\right) \times {}_1F_1\left(\frac{i}{ka_B};1;\frac{kr-\mathbf{k}\cdot\mathbf{r}}{ka_B}\right)\right]. \tag{74}$$

wherein $\Gamma(z)$ is the Gamma function and ${}_1F_1(\xi;\zeta;z)$ the confluent hypergeometric function. If $r \to 0$, then

$$|\psi_{\mathbf{k}}(0)|^2 = \frac{(2\pi e^2/\hbar v)}{1 - exp(-(2\pi e^2/\hbar v))}\ . \tag{75}$$

The non-relativistic average, employing Eqs. (72), (73) and (75), has been computed -as by Bahcall [37]: $(v \ll c)$; i.e.

$$\bar{n}_T = \frac{2\pi e^2 n}{\hbar}\left\langle\frac{1}{v}\right\rangle = n\left(\frac{e^2}{\hbar}\right)\sqrt{\frac{2\mu}{\pi k_B T}}\ . \tag{76}$$

Our final result for the kinetic model of a dilute neutral plasma consisting of electron and protons is the following:

$$\Gamma_T = \left(\frac{4\pi\hbar b}{\mu}\right)\bar{n}_T, b \approx \frac{1}{8\pi^2}\left(\frac{\hbar}{\mu c}\right)\left(\frac{G_F\mu^2}{\hbar c}\right)^2 \times \left(g_V^2 + 3g_A^2\right)\left(\gamma^2 - \gamma^2_{threshold}\right), \tag{77}$$

wherein G_F is the Fermi weak interaction coupling strength, g_V and g_A are respectively the vector and axial vector coupling strengths and

$$\gamma = \left(\frac{m}{m_e}\right); \quad \gamma_{threshold} \sim 2.8 \tag{78}$$

We note in passing that the rate proportional to the inverse velocity occurs both theoretically and experimentally [38] also in the radiative corrections to $p\bar{p}$ annihilation near threshold.

At a physical temperature $T \sim 5000$ K, we recover our original Γ value [29] two orders of magnitude higher for the kinetic model electron capture than that which was incorrectly computed by the Rome group.

Erroneous Maiani screening lengths

Most recently, the Rome group objected to our kinetic calculation on the grounds that we did not include Debye screening lengths into the fully ionized plasma kinetic calculation. An attempt to include Debye was carried out by Maiani et al. [39] who incorrectly found that the Coulomb potential is screened to within less than an Angstrom. This estimate is not sound, since it is very well known [40, 41] that the regime of validity demands that the Debye screening length is valid only if the thermal kinetic energy far exceeds the Coulomb potential energy; i.e.

$$k_B T \gg \frac{e^2}{L} > \frac{e^2}{\Lambda_D}, \tag{79}$$

wherein L is the mean spacing between charged particles and Λ_D is the Debye screening length. At a temperature of $T \sim 5000\ ^oK$, Maiani et al. estimate $\Lambda_D \sim 10^{-8}$ cm which clearly violates the required Eq. (79) by a very large margin. The physical reason why the Rome group estimate for the Debye screening length is incorrect can be stated as follows: For the effective potential between two charges to be screened one must put many other charges between the original two charges. With a screening length on the scale of Angstroms such packing of additional charges is not possible for an electrolytic cell. The remainder of this Appendix is devoted to explaining in more detail, the screened Coulomb potential.

General theory of coulomb screening

If in an overall charge neutral isotropic system there are weak statistical fluctuations in the charge density $\rho(\mathbf{r})$, then due to photon exchange there will be a fluctuation energy

$$U[\rho] = \frac{1}{2}\int\int \rho(\mathbf{r})\rho(\mathbf{r}')\mathbf{V}\left(|\mathbf{r}-\mathbf{r}'|\right)\mathrm{d}^3\mathbf{r}\mathrm{d}^3\mathbf{r}', \tag{80}$$

whence there will be a potential between charges given by

$$V(r) = 4\pi \int \frac{e^{i\mathbf{k}\cdot\mathbf{r}}}{k^2\varepsilon(k)} \left[\frac{d^3\mathbf{k}}{(2\pi)^3}\right]$$
$$V(r) = \frac{2}{\pi}\int \left[\frac{\sin(kr)}{kr}\right] \frac{dk}{\varepsilon(k)}, \tag{81}$$

wherein $\varepsilon(k)$ is the wave number dependent dielectric response function. For the vacuum, the dielectric response function is unity leading to the Coulomb potential $V_{\text{Coulomb}}(r) = 1/r$. For the general condensed matter situation, there will exist a screening function $S(r)$ which modifies the Coulomb potential to

$$V(r) = \frac{1}{r}S(r),$$
$$S(r) = \frac{2}{\pi}\int_0^\infty \sin(kr)\left[\frac{dk}{k\varepsilon(k)}\right]. \tag{82}$$

The wave number dependent dielectric response function may also be found from the screening function via

$$\frac{1}{k\varepsilon(k)} = \int_0^\infty \sin(kr)S(r)dr. \tag{83}$$

The general Coulomb screening length

$$\Lambda = \frac{1}{\kappa} \quad \text{(screening length)} \tag{84}$$

can be defined by either of two limits

$$\varepsilon(k) = 1 + \frac{\kappa^2}{k^2} \quad \text{as} \quad k \to 0,$$
$$S(r) = e^{-\kappa r} \quad \text{as} \quad r \to \infty. \tag{85}$$

Equivalently rigorous formulas for the screening length are

$$\lim_{k\to 0} k^2\varepsilon(k) = \kappa^2, \int V(r)d^3\mathbf{r} = \frac{4\pi}{\kappa^2} = 4\pi\int_0^\infty r^2V(r)dr. \tag{86}$$

The above rigorous results allow for the thermodynamic evaluation of the screening length $\Lambda = \kappa^{-1}$.

Thermodynamic expression for κ

For an uncharged object in the thermodynamic limit of large volumes, the pressure function $P(T, \mu_1, \cdots \mu_f)$ of temperature and chemical potentials represents a complete thermodynamic description via

$$dP = sdT + \sum_{a=1}^{f} n_a d\mu_a \tag{87}$$

wherein s represents the entropy per unit volume and n_a represents the number per unit volume of the a^{th} chemical species with charge $z_a e$. For a mobile electron within the condensed matter system we choose $z_{\text{electron}} = -1$ as the charge convention. For a large sub-volume V of the condensed matter system, the grand canonical ensemble number fluctuation theorem reads

$$\overline{\Delta N_a \Delta N_b} = Vk_BT\left(\frac{\partial^2 P}{\partial\mu_a\partial\mu_b}\right)_T. \tag{88}$$

Since the object is charge neutral we have on average

$$\overline{Q} = e\sum_{a=1}^{f} z_a\overline{N_a} = 0. \tag{89}$$

However the charge does fluctuate according to

$$\overline{Q^2} = e^2\sum_{a=1}^{f}\sum_{b=1}^{f} z_a z_b \overline{\Delta N_a \Delta N_b}. \tag{90}$$

In virtue of Eqs. (88) and (90) one has the charge fluctuation result

$$\overline{Q^2} = k_BTVe^2\sum_{a,b} z_a z_b \left(\frac{\partial^2 P}{\partial\mu_a\partial\mu_b}\right)_T. \tag{91}$$

On the other hand, for a uniform charging of the volume V requires an energy computed from Eq,(80) employing $\rho = (Q/V)$

$$U_Q = \frac{1}{2}\left(\frac{Q^2}{V}\right)\left(\frac{4\pi}{\kappa^2}\right) = \frac{Q^2}{2C_s}, \tag{92}$$

wherein C_s is the self capacitance of the volume; i.e.

$$C_s = \frac{V\kappa^2}{4\pi} \tag{93}$$

and Eq. (86) has been invoked. The Boltzmann factor $\exp(-U_Q/k_BT)$ yields a Gaussian distribution of charge values with dispersion

$$\overline{Q^2} = k_BTC_s = \frac{k_BTV\kappa^2}{4\pi}. \tag{94}$$

Comparing Eqs. (91) and (94), one finds the central result of this section:

Theorem The inverse screening length is determined by the thermodynamic equation of state:

$$\kappa^2 = 4\pi e^2 \sum_{a,b} z_a z_b \left(\frac{\partial^2 P}{\partial \mu_a \partial \mu_b} \right)_T . \tag{95}$$

Depending on the equation of state we have qualitatively different kinds of screening derived from our central theorem. If we take the pressure of degenerate electrons, then we have Thomas-Fermi screening lengths. If the charged particles are dilute and classical, then the screening is that of Debye–Huckel, i.e. for the charge species of particles that are dilute

$$\left(\frac{\partial^2 P}{\partial \mu_a \partial \mu_b} \right)_T = \frac{\delta_{ab} n_a}{k_B T} \qquad \text{(dilute and classical)}, \tag{96}$$

leading to the Debye screening of interest here

$$\kappa^2 = \frac{4\pi e^2}{k_B T} \sum_a z_a^2 n_a . \tag{97}$$

The validity of the *classical* Eq. (97) requires the inequality $k_B T \gg e^2 \kappa$. Hence, the graph presented in their paper is meaningless for most of the densities $[n \geq 10^{18}/cm^3]$ considered there.

Summary

Screening does not appreciably change our previous conclusions on the rates of electron captures in fully ionized plasmas as they appear in physical water cathode surface layers. The Rome group is in disagreement with our results only because they employed the Debye screening length in an unphysical regime of very short screening lengths where the Debye theory does not apply. This is amplified in our discussion of Sect. 7.3.

References

1. Carpinteri A, Borla O, Lacidogna G, Manuello A (2010) Neutron emissions in brittle rocks during compression tests. Phys Mesomech 13:264–274
2. Carpinteri A, Lacidogna G, Manuello A, Borla O (2011) Energy emissions from brittle fracture: neutron measurements and geological evidences of piezonuclear reactions. Strength Fract Complex 7:13–31
3. Carpinteri A, Manuello A (2011) Geomechanical and geochemical evidence of piezonuclear fission reactions in the Earths Crust. Strain Suppl 2(47):267–281
4. Carpinteri A, Chiodoni A, Manuello A, Sandrone R (2011) Compositional and microchemical evidence of piezonuclear fission reactions in rock specimens subjected to compression tests. Strain Suppl 2(47):282–292
5. Carpinteri A, Manuello A (2012) An indirect evidence of piezonuclear fission reactions: geomechanical and geochemical evolution in the Earths crust. Phys Mesomech 15:37–46
6. Carpinteri A, Lacidogna G, Manuello A, Borla O (2012) Piezonuclear fission reactions: evidences from microchemical analysis, neutron emission, and geological transformation. Rock Mech Rock Eng 45:445–459
7. Carpinteri A, Lacidogna G, Borla O, Manuello A, Niccolini G (2012) Electromagnetic and neutron emissions from brittle rocks failure: experimental evidence and geological implications. Sadhana 37:59–78
8. Widom A, Swain J, Srivastava YN (2013) Neutron production from the fracture of piezoelectric rocks. J Phys G Nucl Part Phys G 40:015006–015014
9. Koshevaya S, Grimalsky V, Makarets N, Kotsarenko A, Siquieros-Alatorre J, Perez-Enriquez R, Juarez-Romero D (2008) Electromagnetic emission from magnetite plate cracking under seismic processes. Adv Geosci 14:25–28
10. Swain J, Widom A, Srivastava YN (2013) Electrostrong nuclear disintegration in condensed matter. arXiv:1306.5165 [nucl-th]
11. Widom A, Swain J, Srivastava YN (2013) Photo-disintegration of the iron nucleus in fractured magnetite rocks with magnetostriction. arXiv:1306.6286 [physics gen-phy]
12. Snover KA (1986) Giant resonances in excited nuclei. Annu Rev Nucl Part Sci 36:545–603
13. Brink DM (2008) Giant resonances in excited nuclei. Talk presented at the workshop on chaos and collectivity in many body systems at the PMIPKS, Dresden, 5–8 Mar 2008, pp. 1–5
14. Ishkhanov BS, Kapitonov IM, Varlamov VV (2003) Proceedings of the 10th international seminar electromagnetic interactions of nuclei at low and medium energies, Moscow, 16–18 Apr 2003. Institute for Nuclear Research of the Russian Academy of Sciences, Moscow, pp 5–22. ISBN 5-944274-012-7, 2004
15. Varlamov AV, Varlamov VV, Rudenko DS, Stepanov ME (1999) Atlas of giant dipole resonances: parameters and graphs of photo-nuclear reaction cross sections. International Nuclear Data Committee, INDC(NDS)-394 Distr. GN+NM
16. Liu JC et al (1997) Calculations of the giant dipole resonance photoneutrons using a coupled EGS4 Morse code. Radiat Prot Dosim 70:49–54
17. Mao X et al (1996) Giant dipole resonance neutron yields produced by electrons as a function of target material and thickness. Health Phys 70:207–214
18. Thomas W (1925) ber die Zahl der Dispersionselektronen, die einem stationren Zustande zugeordnet sind. (Vorlufige Mitteilung). Naturwissenschaften 13:627–627
19. Kuhn W (1025) Uber die Gesamtstarke der von einem Zustande aus- gehenden Absorptionslinien. Z Phys 33:408–412
20. Reiche F, Thomas W (1025) Uber die Zahl der Dispersionelektronen die einem stationaren Zustand Zugeordnet sind. Z Phys 34:510–525

21. Migdal AB (1967) Theory of finite Fermi-systems and properties of the atomic nucleus. Willey, New York
22. Migdal AB, Voskresenskii DN, Saperstein EE, Troitskii MA (1990) Pion degrees of freedom in nuclear medium. Phys Rep 192:179–437
23. Berestetskii VB, Lifshitz EM, Pitaevskii LP (1980) Quantum electrodynamics. Pergamon Press, Oxford
24. Lollioz L, Pattofatto S, Hubert O (2006) Application of piezo-magnetism for the measurement of stress during an impact. J Electr Eng 57:15–20
25. Gruerro C, Schelbert J, Bonamy D, Dolmas D (2012) Proc Natl Acad Sci USA 129:190
26. Landau LD, Lifshitz EM (1970) Theory of elasticity. Pergamon Press, Oxford
27. Freund LB (1998) Dynamic fracture mechanics. Cambridge University Press, Cambridge
28. Griffith AA (1921) The phenomena of rupture and flow in solids. Phil Trans R Soc Lond A221:163–197
29. Widom A, Larsen L (2006) Ultra low momentum neutron catalyzed nuclear reactions on metallic hydride surfaces. Eur Phys J C 46:107–112
30. Widom A, Larsen L (2007) Theoretical standard model rates of proton to neutron conversions near metallic hydride surfaces. arXiv:0608059v2 [nucl-th]
31. Cirillo D, Germano R, Tontodonato V, Widom A, Srivastava YN, Del Giudice E, Vitiello G (2012) Water plasma modes and nuclear transmutations on the metallic cathode of a plasma discharge electrolytic cell. Key Eng Mater 495:124–128
32. Cirillo D, Germano R, Tontodonato V, Widom A, Srivastava YN, Del Giudice E, Vitiello G (2012) Experimental evidence of a neutron flux generation in a plasma discharge electrolytic cell. Key Eng Mater 495:104–107
33. Ciuchi S, Maiani L, Polosa AD, Riquer V, Ruocco G, Vignati M (2012) Low energy neutron production by inverse-beta decay in metallic hydride surfaces. Eur Phys J C72:2193–2196
34. Widom A, Srivastava YN, Larsen L (2012) Erroneous wave functions of Ciuchi et al for collective modes in neutron production on metallic hydride cathodes. arXiv:1210.5212v1, [nucl-th]
35. Widom A, Swain J, Srivastava YN (2013) Weak interaction neutron production rates in fully ionized plasmas. arXiv:1305.4899v1, [hep-ph]
36. Flüge S (1970) Practical quantum mechanics. Springer, Berlin
37. Bahcall JH (1962) Electron capture and nuclear matrix elements of Be^7. Phys Rev 128:1297–1301
38. Bardin G et al (1994) Determination of the electric and magnetic form factors of the proton in the time-like region. Nucl Phys B411:3–32
39. Maiani L, Polosa AD, Riquer V (2014) Neutron production rates by inverse-beta decay in fully ionized plasmas. Eur Phys J C 74:2843–2852
40. Abrikosov AA, Gorkov LP, Dzyaloshinskii IE (1975) Methods of quantum field theory in statistical physics, Sect. 22. Dover Publications, New York
41. Landau LD, Lifsitz EM (1981) Fisica Statistica, Sect. 85, vol II. Editori Reuniti Edizioni Mir, Rome